International Journal Of
Industrial Electronics Control and Optimization
Print ISSN: 3517-2645
Online ISSN: 3568-2645
Homepage: https://ieco.usb.ac.ir/

A Mathematical Framework for Designing Precise RBW Filters Using Standard Implementation Techniques in EMI Applications

Seyed Fariborz Zarei[1*] | Saeed Hasanzadeh[1]

Department of Electrical and Computer Engineering, Qom University of Technology, Qom, Iran.[1]

Corresponding author's email: zarei@qut.ac.ir

Article Info

Article type:
Research Article

Article history:
Received: 2025-03-22
Received in revised form: 2025-07-24
Accepted: 2025-07-30
Published online: 2025-09-13

Keywords:
CISPR-16 standard,
Conducted Emissions,
Electromagnetic Interference,
Filter design,
Resolution Bandwidth filters

ABSTRACT

This paper presents a comprehensive approach to the design of Resolution Bandwidth (RBW) filters specifically for Electromagnetic Interference (EMI) applications. We propose a mathematical modeling method that accurately captures the characteristics of standard RBW filters, which are essential for precise EMI noise measurements. The proposed approach utilizes paired complementary second-order filters with symmetrical cutoff frequencies to ensure compliance with CISPR-16 standards. The methodology underscores the importance of aligning theoretical models with real-world filter behavior, ensuring that the resulting models are both accurate and reliable. By establishing a robust framework for RBW filter design, the method enables optimized EMI system performance and the implementation of appropriate filtering solutions. Validation is carried out through simulations using a 150 kHz signal with a dynamically ramped amplitude increase, demonstrating high accuracy and strong performance under both transient and steady-state conditions. Despite the challenging test scenarios, the results confirm that the proposed filter model remains accurate and effective even under worst-case EMI conditions.

I. Introduction

The rapid proliferation of power electronic systems in areas such as renewable energy, electric vehicles, and wireless communications has significantly increased the need for effective Electromagnetic Interference (EMI) management to ensure reliable operation and compliance with standards such as CISPR-16. Resolution Bandwidth (RBW) filters play a crucial role in accurate EMI measurements; however, their design remains challenging in the context of modern, high-frequency systems. Recent studies on modular multilevel converters [1], gate driver optimization [2], and inverter-based networks [3] emphasize the persistent challenges associated with EMI. At the same time, advancements in high-efficiency converters [4], portable resonant chargers [5], and antenna designs incorporating artificial magnetic conductors [6] further highlight the need for precise filter modeling to effectively mitigate EMI in increasingly complex and compact systems.

Electromagnetic interference (EMI) presents significant challenges for power electronic converters, particularly as these systems become increasingly integrated into diverse applications such as renewable energy technologies and electric vehicles [7, 8]. The study of EMI is critical, as it directly affects the reliability, safety, and performance of power electronic devices. Effective management of conducted EMI is essential to ensure that these devices operate within acceptable limits and do not negatively impact surrounding equipment. A fundamental aspect of addressing EMI involves the accurate modeling of measurement components, which serves as the foundation for developing efficient mitigation strategies [9]. Precise modeling enables engineers to predict EMI behavior, optimize filter designs, and enhance overall system performance. As highlighted in various studies [10, 11], modern power electronic converters often operate at higher switching frequencies, which exacerbate both conducted and radiated EMI, necessitating more advanced modeling techniques for effective suppression [9]. Furthermore, the integration of innovative designs and materials, as discussed in [12], underscores the need for tailored EMI mitigation strategies to ensure safe and reliable operation across a broad range of applications. As the demand for high-performance power electronics continues to grow, understanding and mitigating EMI through robust and accurate modeling techniques becomes increasingly critical.

Research in the field of Electromagnetic Interference (EMI) has evolved significantly, with a growing focus on diverse modeling approaches and practical applications. For instance, [13] emphasizes the role of passive filters—particularly EMI filtering chokes—which are essential for noise mitigation and performance optimization in power electronic systems. This study highlights the need for systematic simulation and characterization methods to refine filter design. Similarly, [14] introduces a unified methodology for developing compact EMI

filters tailored to high-frequency switched-mode power converters, stressing the importance of optimizing differential-mode (DM) filter stages for higher power densities while managing common-mode (CM) noise through detailed mathematical modeling. Reference [15] provides a comparative analysis of noise emissions across various converter topologies, clarifying how DM and CM noise characteristics influence filter design strategies. Time-domain simulation techniques, as explored in [16], reveal nonlinear circuit behaviors influenced by resolution bandwidth settings. Advanced models for dual three-phase active bridge rectifiers presented in [17] incorporate conducted EMI noise predictions to enhance filter design for high-power systems while ensuring compliance with international standards. Stabilization strategies for point-of-load converters with integrated EMI filters, discussed in [18], address voltage oscillations caused by LC filter interactions through active damping techniques to improve system stability. The mechanisms of radiated EMI, as analyzed in [12], account for switching behavior, PCB layout, and shielding—factors that are critical in mitigating interference in high-frequency power electronics. In the context of grid-tied solar inverters, [19] proposes filter designs that account for ground leakage currents and component tolerances, ensuring standard compliance while minimizing conducted emissions. Measurement-based equivalent circuit models derived from S-parameters, discussed in [20], have also proven effective in time-domain simulation of EMI filters. Further advancements include innovative algorithms for wide band-pass filter construction [21] and two-phase scanning models for EMI receiver simulations [22], both of which broaden analytical capabilities. Dithering techniques applied to voltage source inverters, as shown in [23], demonstrate how switching frequency modulation can effectively reduce conducted emissions while optimizing system cost and footprint. Methods for DM noise prediction in grid-tied inverters [24] offer high-accuracy analysis of low-frequency EMI up to 150 kHz, while frequency jittering optimization in [25] balances peak and average noise suppression. Finally, the use of artificial neural networks (ANNs) in [26] provides an efficient means of modeling and optimizing EMI filters, highlighting the growing role of intelligent algorithms in EMI management.

Collectively, these studies underscore the critical role that advanced modeling techniques play in addressing the multifaceted challenges posed by EMI in power electronic systems. In this context, the accurate modeling of measurement devices is of paramount importance. Because the output of these devices is evaluated against standardized limits, their faithful representation—aligned with standard-defined characteristics—directly influences the accuracy of EMI assessments and, by extension, the effectiveness of mitigation strategies. Precise models of measurement devices enable more reliable EMI analysis, supporting the development of EMI filters that are not only effective but also optimized in terms of cost, size, and performance. Existing RBW filter designs, such as those based on high-order Butterworth filters, often involve complex tuning procedures to comply with CISPR-16 standards and impose high computational costs. The proposed approach addresses these limitations by employing a simpler, standard-compliant structure based on paired second-order filters. To address these challenges, this paper proposes a novel approach for modeling Resolution Bandwidth (RBW) filters—key components in EMI measurements—using a mathematical framework grounded in standard implementations for EMI applications. This framework is designed to bridge the gap between theoretical models and practical EMI filter design, ensuring both accuracy and compliance with established standards.

The remainder of this paper is organized as follows: Section II provides an overview of the EMI measurement process, highlighting the critical components and procedures involved. Section III introduces the proposed mathematical framework for accurately modeling RBW filters, including detailed methodology and implementation. Section IV presents numerical results that demonstrate the effectiveness and precision of the proposed approach. Finally, Section V concludes the paper with a summary of findings and potential directions for future work.

II. An Overview of the EMI Measurement Circuit

Previous studies have extensively investigated conducted EMI modeling using both time-domain and frequency-domain (spectral) approaches. For accurate simulation of conducted EMI levels, it is essential to model the entire measurement setup in accordance with electromagnetic compatibility (EMC) standards. This section provides a concise overview of the modeling of two critical components within the measurement system: the Line Impedance Stabilization Network (LISN) and the EMI receiver. Notably, the RBW filter—central to this study—is an integral part of the EMI receiver.

A. LISN/AMN

Functioning either as a Line Impedance Stabilization Network (LISN) or, under more recent IEC standards, as an Artificial Mains Network (AMN), this component serves three essential functions: (a) providing high-frequency isolation between the power converter and the power source, (b) maintaining a consistent impedance for both line and ground currents, and (c) ensuring reproducible measurement conditions. A representative LISN circuit, compliant with CISPR 16 requirements for frequencies above 9 kHz, is illustrated in Fig. 1. The voltage representing conducted electrical noise, denoted as u_{noise}, is measured in the time domain. The 50 Ω resistor models the input impedance of the EMI receiver.

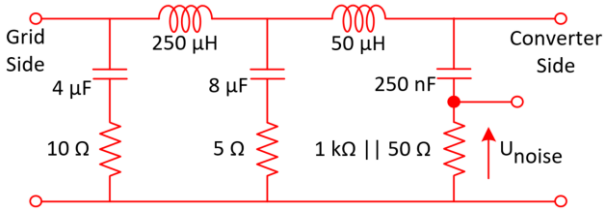

Fig. 1 Circuit diagram of LISN/AMN according to CISPR16 standards

B. EMI Receiver

The second essential component for EMI prediction is the EMI receiver model. As illustrated in Fig. 2, this model represents the general structure of a typical EMI receiver [27]. However, accurately modeling this component presents significant challenges, primarily because manufacturers often do not disclose detailed internal specifications. Consequently, simplified models are commonly employed in the literature as practical alternatives to detailed representations [27].

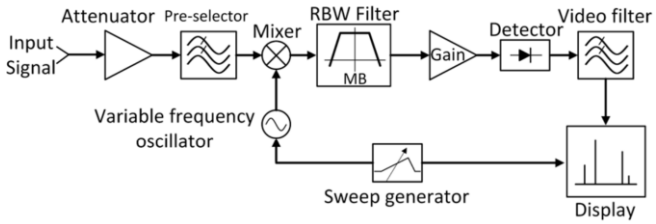

Fig. 2 overall representation diagram of the EMI receiver with different components [27]

C. Resolution Bandwidth (RBW) Filter

The band-pass filter—commonly known as the Resolution Bandwidth (RBW) filter—plays a critical role in determining the extent of EMI emissions captured during measurement. When applied to the voltage spectrum at the output of the LISN, the RBW filter directly influences the measured results. The filter's bandwidth, denoted as BW_{RBW}, is selected based on the frequency range being evaluated, in accordance with standardized guidelines. For the two primary CISPR-defined frequency bands—Band A (9–150 kHz) and Band B (150 kHz–30 MHz)—the corresponding RBW filter bandwidths are 200 Hz and 9 kHz, respectively. Figures 3(a) and 3(b) depict the upper and lower amplitude limits of the RBW filter response for Band A and Band B, respectively, as specified by the CISPR 16 standard.

III. Proposed Model of RBW-Filter and Design Procedure

In the previous section, the various components of the EMI measurement circuit were described. In this section, the proposed RBW filter is introduced, and the design procedure is presented in detail. Additionally, the filter's compliance with the CISPR-16 standard limits is thoroughly discussed.

A. Funfamentals of the Proposed Approach

With reference to Fig. 3 in Section III, the upper and lower bounds specified by the CISPR-16 standard highlight the limitations of conventional first- and second-order filters in meeting standard compliance. Specifically, two primary challenges arise in the implementation of RBW filters: achieving a sufficiently flat response around the mid-band frequency and ensuring compliance with the upper and lower attenuation limits across the remaining frequency range. To address these issues, more complex designs—such as the Butterworth filter—have been proposed in the literature [27]. However, such solutions complicate the mathematical modeling process and increase implementation complexity.

In contrast, this paper proposes a simple yet effective structure based on conventional second-order filters that achieves compliance with CISPR-16 requirements. The proposed method employs two pairs of filters, with each pair consisting of two complementary second-order filters. These filters share the same gain and quality factor but have distinct cutoff frequencies that are symmetrically placed around the center frequency. This configuration ensures that the resulting RBW filter exhibits the required flat mid-band response and adheres to standard roll-off constraints, while maintaining a mathematically tractable and computationally efficient structure.

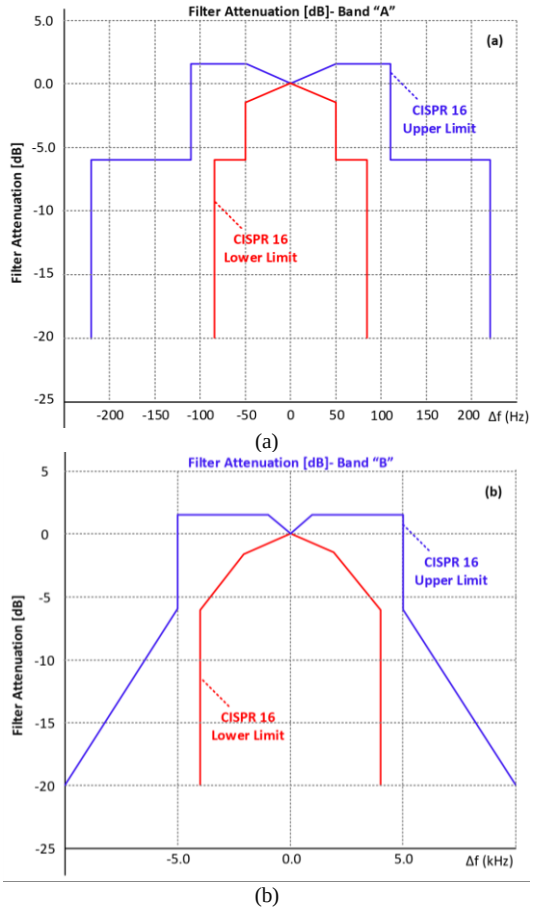

Fig. 3 overall representation diagram of the EMI receiver with different components

To clarify further, Fig. 4 illustrates the conceptual structure of the proposed RBW filter, designed in compliance with the CISPR-16 standard. As shown, the configuration consists of four band-pass filters connected in series. Each filter pair operates in a complementary manner to form the overall standard-compliant RBW filter response. The first two filters are centered at frequencies $f_0 \pm f_1$, and their mathematical formulation is provided in Equations (1) and (2). The resulting frequency response of this filter pair is depicted in Fig. 5(a). As shown, the amplification and attenuation characteristics of the individual filters effectively cancel each other out, yielding a combined response indicated by the dotted line in Fig. 5(a).

$$F_1 = G_1.\frac{2\xi\omega_{n1}s}{s^2 + 2\xi\omega_{n1}s + \omega_{n1}^2} \quad \omega_{n1} = 2\pi.(f_0 + f_1) \qquad (1)$$

$$F_2 = G_2.\frac{2\xi\omega_{n2}s}{s^2 + 2\xi\omega_{n2}s + \omega_{n2}^2} \quad \omega_{n2} = 2\pi.(f_0 - f_1) \qquad (2)$$

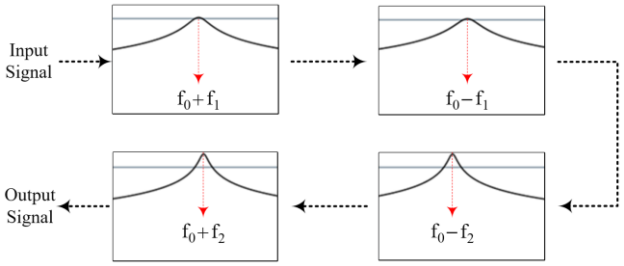

Fig. 4 Conceptual representation of the proposed RBW-filter structure compliant with the CISPR-16 standard

Similarly, the second pairs of the filters given in Fig. 4 are tuned on the frequency of $f_0 \pm f_2$ with $f_2 > f_1$. Fig. 5 (b) shows the resultant frequency characteristics of this pair of band-pass filters. The same equations of (1)-(2) can be defined for this pairs of filters, shown in (3)-(4). The simultaneous amplification and attenuation of the amplitudes of these filters compensate each other and produces the characteristics shown by dotted line in Fig. 5 (b).

$$F_3 = G_3.\frac{2\xi\omega_{n3}s}{s^2 + 2\xi\omega_{n3}s + \omega_{n3}^2} \quad \omega_{n3} = 2\pi.(f_0 + f_2) \qquad (3)$$

$$F_4 = G_4.\frac{2\xi\omega_{n4}s}{s^2 + 2\xi\omega_{n4}s + \omega_{n4}^2} \quad \omega_{n4} = 2\pi.(f_0 - f_2) \qquad (4)$$

Combining the two pair filters results in a filter with standard characteristics shown in Fig. 5 (c).

B. Design of a Sample RBW Filter

To exemplify the proposed structure for the RBW filter, a design example dedicated for power electronics application in power grid is presented in this section.

1- *The First Pair of Filters*:

The base frequency of 150 kHz is considered for this example. The frequency deviation of f_1= 2 kHz is chosen for this study. The resultant filter gain and quality factor ($=\frac{1}{2\xi}$) are determined 1.08 and 13.5, respectively. The two filters in this pair, and the resulted output filter, dotted line, are given in Fig. 5 (a).

2- The Second Pair of Filters:

The base frequency of 150 kHz is considered for this case. The frequency deviation of f_1= 5 kHz is chosen for this part. The resultant filter gain and quality factor ($=\frac{1}{2\xi}$) are determined 2.4 and 32.7, respectively. The two filters in this pair, and the resulted output filter, dotted line, are given in Fig. 5 (b).

The resulted filter is given in Fig. 5 (c), in which its fundamental parts $F_1 \times F_2$ and $F_3 \times F_4$ filters, shown respectively by red and blue waveform characteristic. These two filters together with each other results in a dotted line filter given in this figure. As shown in this figure, the dotted line filter has a flat characteristic in the base frequency, and the filter bandwidth is 9 kHz, which is within the standard region highlighted by cyan color in this figure.

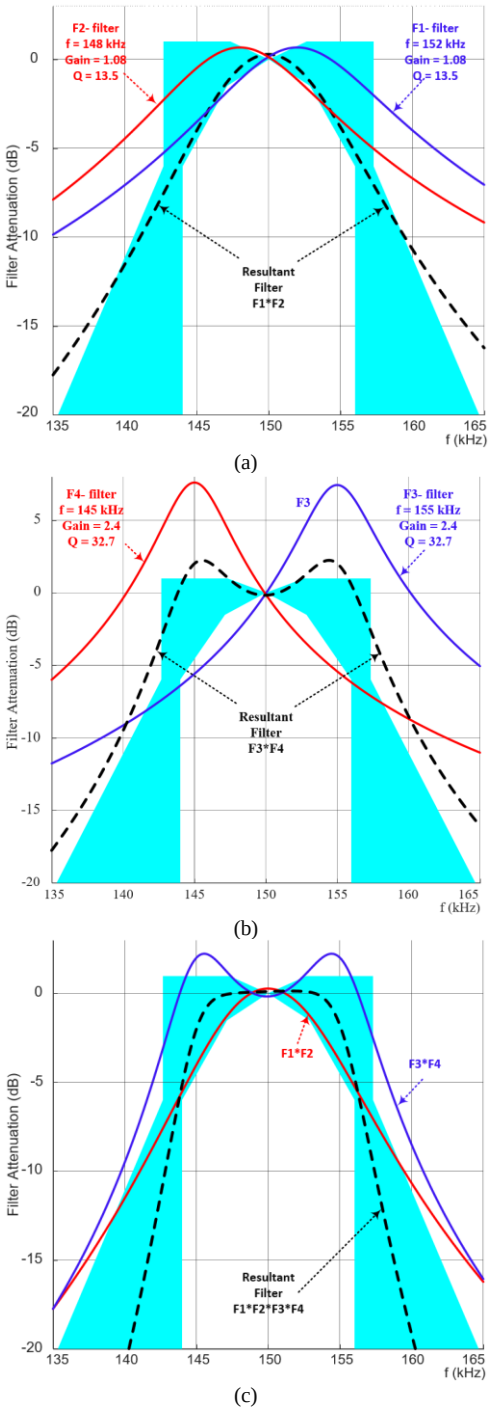

Fig. 5 overall representation diagram of the EMI receiver with different components

The gains (G_1 = 1.08, G_3 = 2.4) and quality factors (Q_1 = 13.5, Q_3 = 32.7) for the first and second filter pairs were optimized via iterative simulations to achieve a 9 kHz bandwidth and flat

passband meeting CISPR-16 standards, as shown in Fig. 5 (c). The first pair ensures passband flatness around 150 kHz, while the second pair enhances roll-off and bandwidth control. Higher Q values improve selectivity but increase sensitivity to parameter variations, which was balanced to ensure robust performance.

3- *Implementation of the RBW Filters*:

To implement the RBW filters in practical applications, it is essential to utilize their discrete-time transfer functions. In this work, the backward Euler discretization method is adopted to maintain simplicity and avoid unnecessary computational complexity. This method approximates the derivative using two consecutive signal samples, enabling straightforward real-time implementation. By applying this approach, Equation (5) yields the discrete form necessary for realizing the proposed RBW filters in digital systems.

$$F_i(z) = G_i.\frac{\omega_{ni}.T_s}{Q_i}.\frac{1-z^{-1}}{b_0 + b_1.z^{-1} + z^{-2}}$$

where,

$$b_0 = 1 + \frac{\omega_{ni}.T_s}{Q_i} + (\omega_{ni}.T_s)^2 \qquad (5)$$

$$b_1 = -2 - \frac{\omega_{ni}.T_s}{Q_i}$$

$$i = 1 \sim 4$$

In this equation, the subscript "i" ranges from 1 to 4, corresponding to the filter numbering F1–F4 of (1)-(4). Also, ω_{ni} is the cutoff frequency (rad/s) for filters F1–F4, and T_s is the sample time.

The backward Euler method was selected to discretize Equation (5) due to its simplicity and unconditional stability, making it well-suited for real-time implementation. This method requires only 12 multiplications per sample, contributing to computational efficiency without compromising performance. For the 150 kHz RBW filter, it achieves 100% steady-state accuracy, as demonstrated in Fig. 6. At higher operating frequencies, such as 30 MHz, minor frequency warping may occur—resulting in a center frequency shift of less than 1%. This distortion can be mitigated by increasing the sampling rate to 2 MHz. While alternative discretization techniques, such as the bilinear transformation, offer more precise frequency mapping, they come at the cost of increased computational complexity.

The proposed RBW filter structure employs symmetrical cutoff frequencies to ensure a balanced frequency response aligned with the flat mid-band and steep roll-off characteristics required by CISPR-16 standards (see Fig. 3). This symmetry simplifies the design by ensuring that the amplification and attenuation effects of each filter pair—defined by Equations (1)–(4)—cancel each other appropriately outside the target passband. As a result, the filter exhibits a response that conforms to standard specifications, such as the 9 kHz bandwidth required for Band B. The filter configuration was analytically derived by setting the cutoff frequencies symmetrically around the center frequency (e.g., 150 kHz in the design example), enabling a flat band-pass response and controlled roll-off, as shown in Fig. 5(c).

It is important to note that asymmetric cutoff frequency configurations were evaluated during the design process. However, these designs produced undesirable band-pass ripples and insufficient stopband attenuation, failing to satisfy CISPR-16 criteria. In contrast, the symmetrical approach leverages the complementary behavior of filter pairs to achieve a flat passband (within ±0.5 dB) and strong stopband rejection, as illustrated in Fig. 5(c). Moreover, this configuration simplifies tuning and reduces computational overhead, reinforcing the practical advantages of the proposed methodology.

IV. Simulation Results

In this section, the performance of the proposed RBW filter is validated through time-domain simulations conducted in MATLAB/Simulink. A 150 kHz test signal is applied, with its amplitude increasing linearly via a ramp function at a slope of 0.25 V/s. The signal reaches its steady-state condition at approximately 4.0 seconds, as illustrated by the blue trace labeled "Original Signal" in Fig. 6. This input is processed using the proposed filter configuration shown in Fig. 5, and the corresponding filtered output is presented as the red trace in Fig. 6. To enable detailed waveform analysis, Figs. 6(a) through 6(e) display zoomed-in views of the signal at different time intervals. Visual inspection of these plots confirms a strong alignment between the original and filtered signals. Fig. 7 compares the amplitudes of the original and filtered signals, clearly demonstrating the close tracking achieved by the proposed RBW filter. Fig. 8 quantifies the percentage error between the amplitudes of the original and filtered signals. The error remains consistently below 0.02 per unit (p.u.) throughout both the transient and steady-state periods. Notably, the highest error values occur in the low-amplitude region; however, the error decreases to below 3% once the input signal amplitude exceeds 0.6 p.u.

These results confirm that the proposed RBW filter maintains high accuracy even during dynamic amplitude transitions. Specifically, the filter's accuracy improves significantly after t=2.5 seconds, when the input amplitude surpasses 60%, and reaches 100% accuracy under steady-state conditions beyond 4.0 seconds, as depicted in Fig. 8. It is important to highlight that, in practical EMI measurement scenarios, steady-state behavior is of primary importance, as dynamic conditions are not typically considered standard criteria for assessment. Nevertheless, dynamic amplitude changes serve as stringent test conditions, challenging the stability and accuracy of amplitude extraction methods. The strong performance of the proposed RBW filter under such conditions underscores its robustness and reliability.

It is also worth noting that the proposed 8th-order RBW filter, which requires only 12 multiplications per sample due to its paired second-order structure, achieves 100% steady-state accuracy and less than 3% error during transient conditions for a 150 kHz signal, as shown in Fig. 6. In contrast, a fourth-order Butterworth filter—while requiring fewer operations (8 multiplications per sample) and offering comparable passband flatness—features a less steep roll-off and increased complexity when scaled to higher orders to meet CISPR-16 requirements.

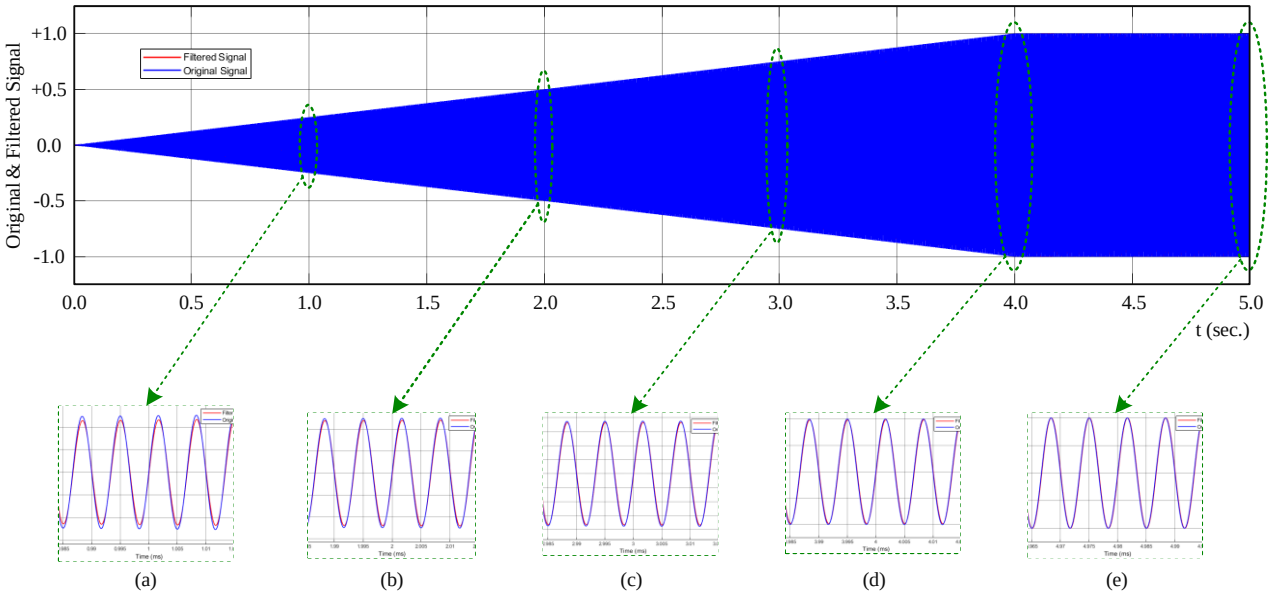

Fig. 6 the 150 kHz signal with ramp increase in the amplitude with the ramp rate of 0.25 volts/sec., signal waveforms shown in (a) to (e) corresponding to time slots of 1.0, 2.0, 3.0, 4.0, and 5.0 seconds, respectively.

The simpler tuning and high accuracy of the proposed approach thus offer a favorable trade-off between computational efficiency and regulatory compliance.

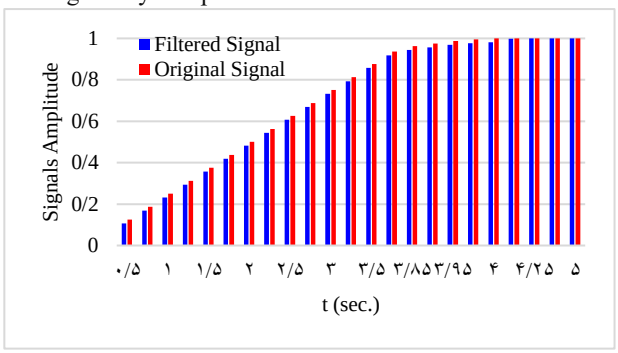

Fig. 7 the amplitudes of original and the filtered signals shown in Fig. 6, showing close proximity of these signals using the proposed RBW-filter

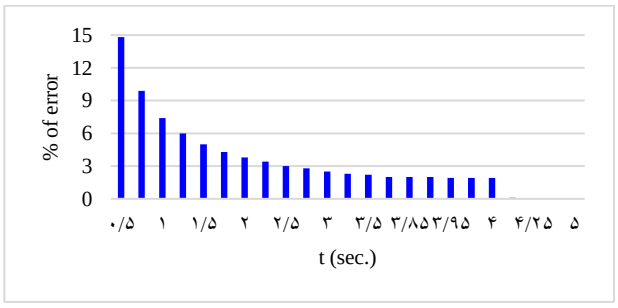

Fig. 8 the percent of error between amplitudes of original and the filtered signals shown in Fig. 6, showing the improved performance during higher amplitudes and under the steady-state region.

V. Conclusions

This paper presents a comprehensive approach to the design of Resolution Bandwidth (RBW) filters for Electromagnetic Interference (EMI) applications, addressing key challenges in modern measurement systems. The proposed structure employs paired complementary second-order filters with symmetrical cutoff frequencies (e.g., $f_0 \pm f_1$ and $f_0 \pm f_2$), achieving full compliance with CISPR-16 requirements while maintaining computational simplicity. Filter performance is validated through simulations using a 150 kHz signal with a dynamically ramped amplitude, demonstrating 100% accuracy under steady-state conditions. Additionally, the filter exhibits a robust dynamic response, achieving over 97% accuracy when the signal amplitude exceeds 60%. This methodology not only offers a practical and reproducible framework for developing standard-compliant RBW filters but also balances mathematical rigor with real-world applicability, making it a valuable tool for engineers engaged in EMI mitigation strategies.

VI. Acknowledgment

Acknowledge the use of Perplexity AI (https://www.perplexity.ai) to enhance the clarity and language of the manuscript. The tool was used solely for checking sentence grammar and writing during the drafting phase. All suggestions and generated content were critically reviewed and edited by the authors to ensure compliance with academic standards.

References

[1] M. Rahmani, S. M. Barakati, S. Yousofi Darmian, V. Barahouei, and M. Bagheri Hashkavayi, “Optimized algorithm for open-circuit fault detection in switches and capacitor voltage balancing control in modular multilevel converters,” International Journal of Industrial Electronics Control and Optimization, vol. 7, no. 1, pp. 15-27, 2024.

[2] S. Ahmadi, K. Khalaj Monfared, M. Khalilzadeh, and H. Imaneini, “A Technical Review on the Proper Design of Gate Drivers in Industrial Power Electronics Applications,” International Journal of Industrial Electronics Control and Optimization, vol. 7, no. 2, pp. 109-117, 2024.

[3] M. Behbahanipour, S. F. Zarei, and M. Shateri, "Impedance-Based Approach for Locating Short-Circuit Faults in Inverter-Based Active Distribution Networks," International Journal of Industrial Electronics Control and Optimization, vol. 7, no. 3, pp. 225-233, 2024.

[4] H. A. H. Al-Ameedee, M. Delshad, N. A. Shalash, and B. Fani, "A new soft switching dual-input high step-up converter for renewable energy systems," International Journal of Industrial Electronics Control and Optimization, vol. 8, no. 2, pp. 211-219, 2025.

[5] J. Shahsevani and R. Beiranvand, "A Compact, High Efficiency, and Portable Wireless EV Resonant Charger," International Journal of Industrial Electronics Control and Optimization, vol. 8, no. 2, pp. 137-148, 2025.

[6] H. Malekpoor and M. Hamidkhani, "Radiation Improvement of Low-Profile Microstrip Antenna by Utilizing AMC Surface for MIMO and Wireless Systems," International Journal of Industrial Electronics Control and Optimization, vol. 8, no. 2, pp. 129-136, 2025.

[7] S. F. Zarei, M. A. Ghasemi, S. Peyghami, P. Davari, H. Mokhtari, and F. Blaabjerg, "Characterization of proportional-integral-resonant compensator for DC link voltage control," in 2018 IEEE 19th Workshop on Control and Modeling for Power Electronics (COMPEL), 2018: IEEE, pp. 1-8.

[8] M. A. Ghasemi, M. Parniani, S. F. Zarei, and H. M. Foroushani, "Fast maximum power point tracking for PV arrays under partial shaded conditions," in *2016 18th European Conference on Power Electronics and Applications (EPE'16 ECCE Europe)*, 2016: IEEE, pp. 1-12.

[9] S. F. Zarei and S. Khankalantary, "A simplified frequency model for industrial common-mode chocks used in high-power converters," *Journal of Electromagnetic Engineering and Science*, vol. 21, no. 1, pp. 15-22, 2021.

[10] L. Yuan, J. Zhang, Z. Liang, M. Hu, G. Chen, and W. Lu, "EMI challenges in modern power electronic-based converters: recent advances and mitigation techniques," *Frontiers in Electronics*, vol. 4, p. 1274258, 2023.

[11] Z. Zhang, Y. Hu, X. Chen, G. W. Jewell, and H. Li, "A review on conductive common-mode EMI suppression methods in inverter fed motor drives," *IEEE Access*, vol. 9, pp. 18345-18360, 2021.

[12] Z. Ma, Y. Lai, Y. Yang, Q. Huang, and S. Wang, "Review of radiated EMI modeling and mitigation techniques in power electronics systems," in *2023 IEEE Applied Power Electronics Conference and Exposition (APEC)*, 2023: IEEE, pp. 1776-1783.

[13] H. Jie, Z. Zhao, H. Li, C. Wang, Y. Chang, and K. Y. See, "Characterization and Circuit Modeling of Electromagnetic Interference Filtering Chokes in Power Electronics: A Review," *IEEE Transactions on Power Electronics*, 2024.

[14] S. Dey, A. Mallik, and S. Mishra, "A mathematical design approach to volumetric optimization of EMI filter and modeling of CM noise sources in a three-phase PFC," *IEEE Transactions on Power Electronics*, vol. 37, no. 1, pp. 462-472, 2021.

[15] D. Zhang, M. Leibl, J. Muhlethaler, J. Huber, and J. W. Kolar, "Analytical Modeling and Comparison of EMI Pre-Filter Noise Emissions of Three-Phase Voltage and Current DC-Link Converters," *IEEE Transactions on Power Electronics*, 2024.

[16] S. Negri, G. Spadacini, F. Grassi, and S. A. Pignari, "Prediction of EMI filter attenuation in power-electronic converters via circuit simulation," *IEEE Transactions on Electromagnetic Compatibility*, vol. 64, no. 4, pp. 1086-1096, 2022.

[17] M. J. Heller, F. Krismer, and J. W. Kolar, "EMI filter design for the integrated dual three-phase active bridge (D3AB) PFC rectifier," *IEEE Transactions on Power Electronics*, vol. 37, no. 12, pp. 14527-14546, 2022.

[18] R. Kumar and C. N. Bhende, "Model predictive control-based voltage oscillations stabilizer for point-of-load converter with EMI filter in DC microgrids," *IEEE Journal of Emerging and Selected Topics in Industrial Electronics*, 2024.

[19] H. Hizarci, U. Pekperlak, and U. Arifoglu, "Conducted emission suppression using an EMI filter for grid-tied three-phase/level T-type solar inverter," *IEEE Access*, vol. 9, pp. 67417-67431, 2021.

[20] S. Negri, G. Spadacini, F. Grassi, and S. Pignari, "Measurement-based equivalent circuit model for time-domain simulation of EMI filters," in *2022 International Symposium on Electromagnetic Compatibility–EMC Europe*, 2022: IEEE, pp. 793-798.

[21] D. Nesic and T. Milosevic, "Application of a New Algorithm for the Wide Bandpass Filters," in *2021 15th International Conference on Advanced Technologies, Systems and Services in Telecommunications (TELSIKS)*, 2021: IEEE, pp. 92-95.

[22] J. Yan, X. Pei, Y. Yu, K. Zhang, and T. Li, "EMI Receiver Modeling Based on Two-phase Scanning Mode," in *2021 IEEE 1st International Power Electronics and Application Symposium (PEAS)*, 2021: IEEE, pp. 1-5.

[23] S. Nayak, V. Pandey, and K. Hatua, "A Dithering Technique for Mitigation of Conducted Emission Noise of SiC MOSFET Based VSI Driving an Induction Motor," *IEEE Transactions on Power Electronics*, 2023.

[24] N. N. Esfetanaj, J. Meyer, H. Wang, F. Blaabjerg, and P. Davari, "Differential mode noise prediction and analysis in single and three phase grid-tied inverters for the frequency range of 9-150 kHz," in *2021 23rd European Conference on Power Electronics and Applications (EPE'21 ECCE Europe)*, 2021: IEEE, pp. 1-10.

[25] Z. Chen, J. Zhang, and S. Shao, "Optimization of Frequency Jittering Parameters for Conducted EMI Suppression in Switching Mode Power Supplies," in *2023 IEEE 3rd International Conference on Industrial Electronics for Sustainable Energy Systems (IESES)*, 2023: IEEE, pp. 1-6.

[26] H. Chen and S. Ye, "Modeling and optimization of EMI filter by using artificial neural network," *IEEE Transactions on Electromagnetic Compatibility*, vol. 61, no. 6, pp. 1979-1987, 2019.

[27] P. Davari, F. Blaabjerg, E. Hoene, and F. Zare, "Improving 9-150 kHz EMI performance of single-phase PFC rectifier," in *CIPS 2018; 10th International Conference on Integrated Power Electronics Systems*, 2018: VDE, pp. 1-6.

Seyed Fariborz Zarei received his B.Sc. in Electrical Engineering from Amirkabir University of Technology (2012) and his M.Sc. and Ph.D. from Sharif University of Technology (2014, 2019). He was a Visiting Ph.D. Scholar at Aalborg University in 2018. Since 2021, he has been with Qom University of Technology, promoted to Associate Professor in 2025. Dr. Zarei has published over 45 papers on power electronics and power grids, focusing on modeling, control, protection, and stability. He founded the Power Electronic and Grid Laboratory in 2022, studying DC/AC converters and their interaction with AC grids through advanced experimental platforms.

Saeed Hasanzadeh earned his B.Sc. from Shahroud University of Technology (2003) and his M.Sc. and Ph.D. from the University of Tehran (2006, 2012), specializing in High Voltage Engineering and Wireless Power Transfer. He joined Qom University of Technology in 2013, became an Associate Professor in 2022, and served as Dean from 2018 to 2023. He is a member of the editorial board of PELSI, IEEE PEDSTC Technical Program Committee, and Scientific Chair of ICREDG2025. He has received top research awards (2019, 2023) and was named Qom Province's top innovator (2023). His research interests include power electronics, electrical machines, WPT, and high voltage engineering.